Chem

CellPress
OPEN ACCESS

Article

Twisted rectangular subunits self-assemble into a ferritin-like capsule

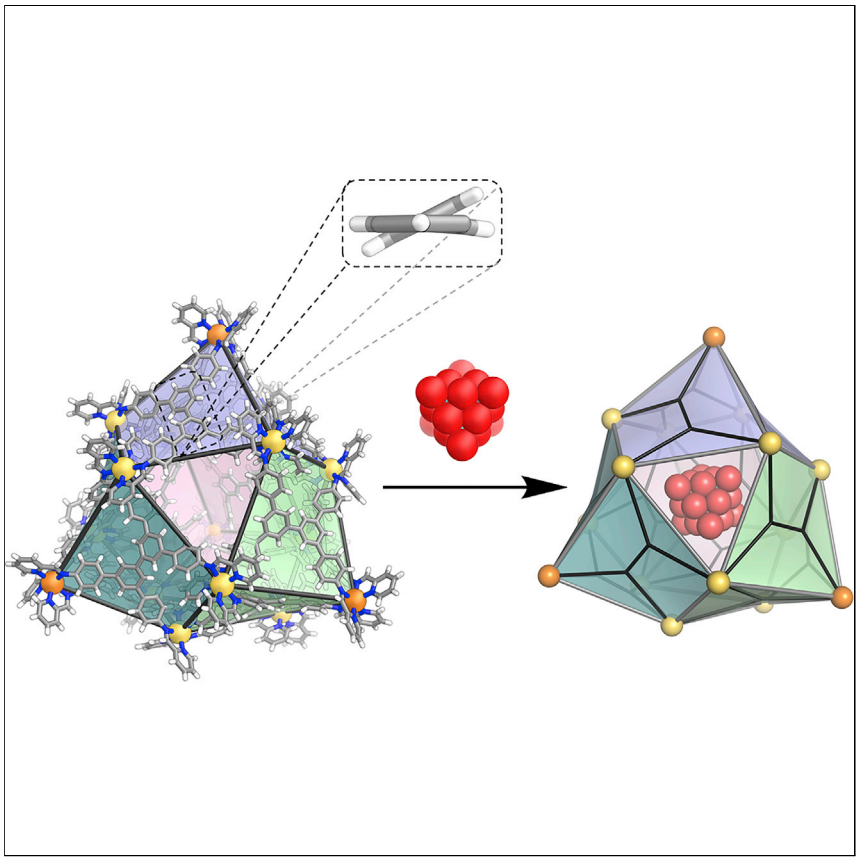

Many molecular capsules used for applications have single ligands defining the edges or faces of a polyhedron, which limits the volume of the interior cavity. Spanning the vertices of a capsule with multiple subunits would allow a given ligand to enclose a greater volume. Herein, we report the self-assembly of a twisted tetramine subcomponent into a tetrahedral metal-organic capsule, with each face of the capsule composed of three ligand panels. The large architecture was observed to bind large dianions.

Jack A. Davies, Tanya K. Ronson, Jonathan R. Nitschke

jrn34@cam.ac.uk

Highlights

Twisted rectangular subcomponents self-assemble into a large tetrahedral architecture

Each triangular face of the tetrahedron is composed of three ligand units

A smaller M_8L_6 cubic assembly forms as an isolable kinetic intermediate

The large host binds multiple equivalents of a large dianionic guest

Davies et al., Chem 8, 1099–1106
April 14, 2022
https://doi.org/10.1016/j.chempr.2022.01.003

Chem

CellPress
OPEN ACCESS

Article

Twisted rectangular subunits self-assemble into a ferritin-like capsule

Jack A. Davies,[1] Tanya K. Ronson,[1] and Jonathan R. Nitschke[1,2,*]

SUMMARY

The vertices of polyhedral protein capsules are spanned by multiple capsule-forming protein subunits, thus enclosing more volume and larger cargoes than if single proteins connected vertices directly. Application of protein cage design principles to synthetic analogs would allow a given ligand to enclose a greater volume. Here, we report the self-assembly of a simple tetramine subcomponent into a tetrahedral metal-organic capsule, with each face of the capsule composed of three ligand panels. The edges of the capsule are 31.8 Å in length—double the distance that can be spanned by a single subcomponent. The self-assembly rules followed by this system are programmed into the tetramine—it twists out of planarity in its lowest-energy configuration, thus favoring the large capsule over a simpler cube-like architecture. Unlike other large metal-organic capsules, the cavity of this new capsule is enclosed, and the structure was observed to bind large dianionic guests.

INTRODUCTION

High-symmetry protein capsules[1] serve to transport and store payloads, from the fragile genetic material of viruses, to the iron within ferritins. The vertices of these polyhedral capsules are spanned by multiple capsule-forming protein subunits.[2,3] In contrast, synthetic polyhedral metal-organic capsules[4,5] with enclosed cavities for binding guests have single ligands that span vertices, limiting the volumes enclosed and the sizes of possible payloads.[6,7]

Foundational work by Fujita,[8–10] Stang,[11,12] and others[5,13–19] provides examples of large metal-organic and purely organic[20–22] architectures assembled from high-symmetry building blocks with carefully chosen geometries. These polyhedra often have regular Platonic or Archimedean geometries, where individual subunits define the faces or edges of the polyhedron. Such structures tend to be porous, with the self-assembled framework defining an inner space without enclosing it for guest binding.

Here, we report the self-assembly of tetramine subcomponent **1** into a large metal-organic capsule, with each face of the polyhedral capsule composed of three ligand panels. The arrangement of the tetramine subunits of this capsule mimics the arrangement of the capsule-forming proteins of *Archaeoglobus fulgidus* ferritin.[24] As with natural protein cages, the symmetry elements of the overall structure do not emerge from the individual subunits, which are in low local-symmetry configurations, but rather from how they come together.[2,26,27] Unlike other large metal-organic capsules,[9–14,19,28] the cavity of this new capsule is enclosed, and the structure was observed to bind multiple equivalents of $Mo_6O_{19}^{2-}$ in solution. Planar rectangular tetramines are known to assemble into M_8L_6 cube-like

The bigger picture

Molecular capsules can catalyze reactions, perform chiral separations, and stabilize reactive molecules. Many of the molecular capsules used for such applications have Platonic geometries—tetrahedral, cubic, and octahedral—with single ligands defining the edges or faces of the polyhedron. This limits the volume of the interior cavity and thus the size of substrates that can be sequestered, stabilized, or transformed.

Here, we report the assembly of a large metal-organic capsule from simple subcomponents. Instead of single ligands spanning its vertices, each face of the tetrahedral capsule is paneled by three ligands, thus leading to a much larger framework than would otherwise be observed. The resulting cavity remains enclosed, and the structure exhibits guest binding. The principles developed herein provide a promising platform for the preparation of other metal-organic architectures with large, enclosed internal volumes.

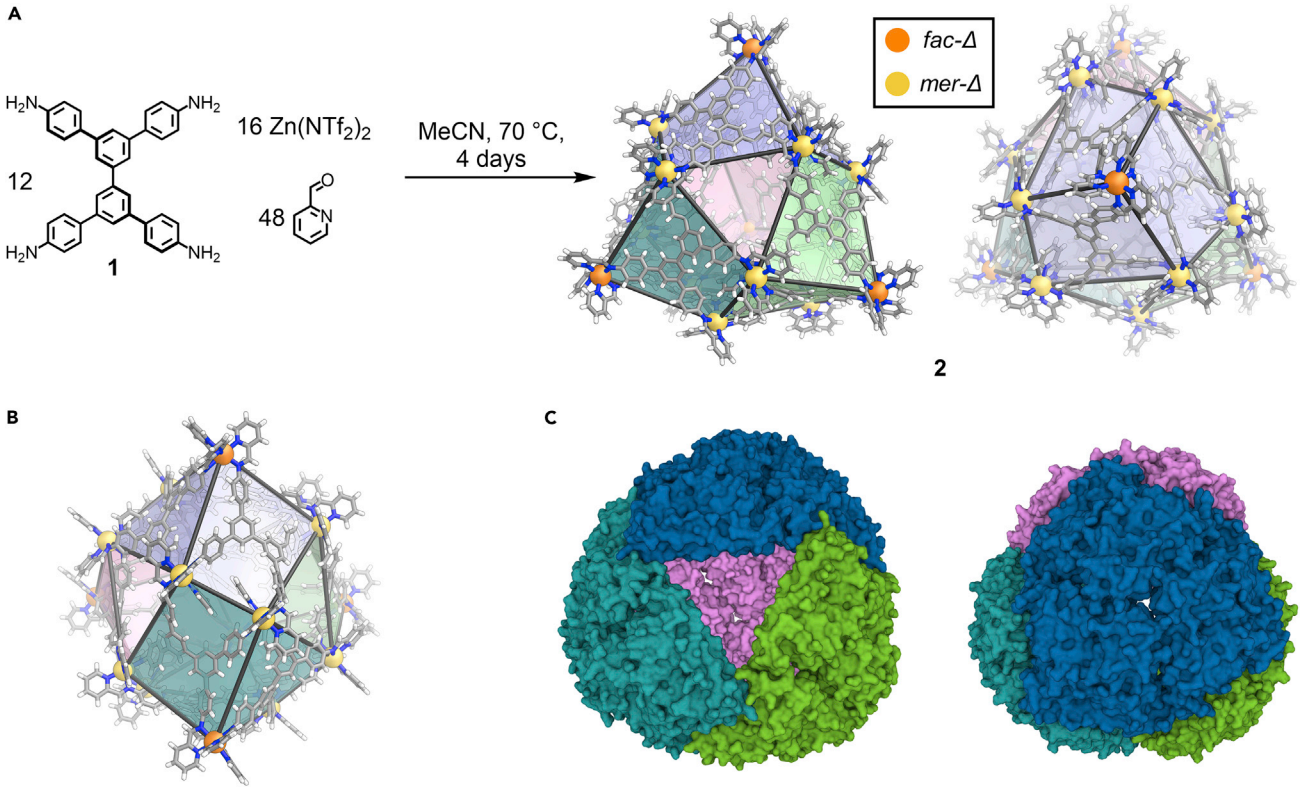

Figure 1. Self-assembly of capsule 2 and its structural resemblance to *Archaeoglobus fulgidus* ferritin

(A) Self-assembly of twisted rectangular subcomponent **1**, 2-formylpyridine, and zinc(II) bis(trifluoromethanesulfonyl)imide into $[Zn_{16}L_{12}]^{32+}$ capsule **2** in acetonitrile.

(B) View of the crystal structure of **2** down a C_2 axis.

(C) Views of the crystal structure of *Archaeoglobus fulgidus* ferritin, with dimeric subunits colored to highlight its isomorphism with **2**.[23–25]

coordination cages.[29–31] Tetra-aniline subcomponent **1** (Figure 1A) has a twisted geometry in its ground state, and it thus does not straightforwardly define the symmetry axis of a polyhedron. We thus hypothesize that the twist in **1** favors the formation of a higher-order assembly.[32]

RESULTS AND DISCUSSION

Synthesis and characterization of 2

Subcomponent **1** reacted with 2-formylpyridine and zinc(II) bis(trifluoromethanesulfonyl)imide in acetonitrile to produce capsule **2** (Figure 1A). The solid-state structure of **2** was determined by single-crystal X-ray diffraction using synchrotron radiation. The $[Zn_{16}L_{12}]^{32+}$ structure of **2** contains four Zn^{II} centers with *facial* (*fac*) stereochemistry, coincident with its C_3 axes, and twelve Zn^{II} ions with a lower-symmetry *meridional* (*mer*) configuration. The presence of lower-symmetry *mer*-configured metal ions enables the formation of larger structures with increased structural complexity,[5,33] as in the present case.

The structure of **2** consists of four "half-cube" units joined together. Each of these units is crowned with a *fac* Zn^{II} center, shown in orange in Figure 1, corresponding to the vertex of a tetrahedron. The four units are shown in different colors in Figure 1. The twisted conformation of the **1** residue within **2** favors an opening out of the faces of these "half-cubes," disfavoring the formation of a smaller architecture. The seams between "half-cubes" are *mer* Zn^{II} centers, shown in yellow in Figure 1. All 16 metal

[1]Yusuf Hamied Department of Chemistry, University of Cambridge, Lensfield Road, Cambridge CB2 1EW, UK

[2]Lead contact

*Correspondence: jrn34@cam.ac.uk

https://doi.org/10.1016/j.chempr.2022.01.003

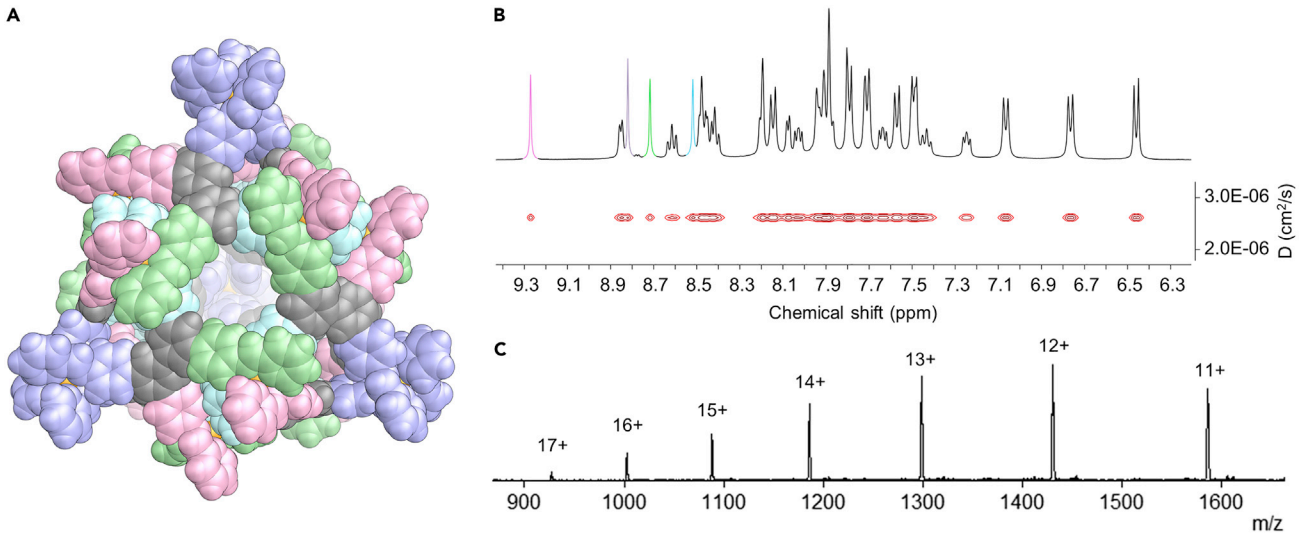

Figure 2. Solid- and solution-state characterization of 2

(A) Crystal structure of **2** viewed down a C_3 axis, with the ligands shown in space-filling mode and each chemically distinct ligand arm colored differently.

(B) Partial ^{1}H NMR and DOSY spectra (400 MHz, CD_3CN, 298 K) of **2**·$(NTf_2)_{32}$, with the four distinct imine proton signals colored to correspond to the view in Figure 2A.

(C) Low-resolution ESI-MS spectrum for **2**.

centers within **2** have the same Δ or Λ handedness, and the relative orientations of the three converging ligands in the "half-cube" units allow the structure to form with minimal strain (Figures S45 and S46).

Capsular structure **2** has overall *T* point symmetry. None of its four C_3 or three C_2 axes are generated by its ligands; each ligand has no internal symmetry within **2**. Its C_3 axes run through the *fac* Zn^{II} centers and are perpendicular to the triangular pores between ligands (Figure 1A). The C_2 axes pass through gaps between the ligands linked by *mer* Zn^{II} centers, as shown in Figure 1B.

The structure of **2** is homologous to that of *Archaeoglobus fulgidus* ferritin (Figure 1C), with the ligands of **2** mapping onto dimeric protein subunits of the ferritin.[24] Comparing the crystal structures of the two capsules (Figures 1A and 1C, respectively) shows this structural homology. Capsule **2** also shows the same symmetry and arrangement of subunits to the Dps[34] (DNA-binding protein from starved cells) dodecamer (Figure S49).

Solution-state data were consistent with the solid-state structure of **2**. Electrospray ionization-mass spectrometry (ESI-MS) data were consistent with a $[Zn_{16}L_{12}]^{32+}$ composition (Figure 2C), and ^{1}H diffusion-ordered spectroscopy (DOSY) data indicated the presence of a single species in solution (Figures 2B and S21), with a solvodynamic radius of 2.5 nm. As expected from its solid-state structure, the ^{1}H NMR spectrum of **2** (Figures 2B, S12, and S13) indicates that each of the four ligand arms is magnetically distinct. Two-dimensional NMR spectra (Figures S16–S20) enabled the assignment of the ^{1}H NMR signals from each arm.

Concentration and reaction-time dependence of the self-assembly process

At a lower **1** concentration of 2.4 mM and a shorter reaction time of 1 day, the smaller structure **3** was isolated (Figure 3) instead of **2**. The solid-state structure of **3** was determined by single-crystal X-ray diffraction using synchrotron radiation. The

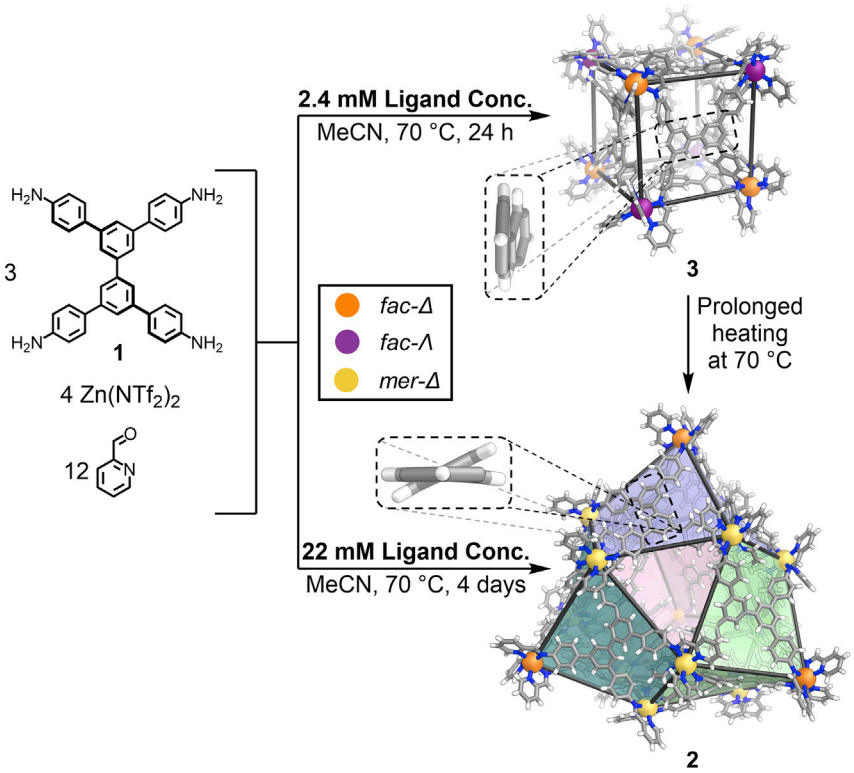

Figure 3. Concentration-dependent formation of 3 versus 2

The assembly of $[Zn_8L_6]^{16+}$ structure **3** and $[Zn_{16}L_{12}]^{32+}$ architecture **2** from subcomponent **1**, 2-formylpyridine, and zinc(II) bis(trifluoromethanesulfonyl)imide in acetonitrile, depending on concentration and reaction time. The central biphenyl moiety of one ligand in each structure is highlighted to illustrate the difference in torsion angles between the two phenyl groups of the central biphenyl unit.

structure of **3** consists of a $[Zn_8L_6]^{16+}$ cube-like architecture, with eight *fac* Zn^{II} centers (Figure 3). Of the eight *fac* Zn^{II} centers in **3**, four have Δ handedness and four Λ, alternating to give rise to T_h point symmetry (Figures 3, S47, and S48). Mass spectrometry (Figures S10 and S11) and NMR spectroscopy (Figures S1–S9) gave results consistent with the X-ray crystal structure of **3**.

Either **2** or **3** can thus be obtained from the same building blocks, depending on concentration and reaction time. Even dilute (158 μM) solutions of **3** slowly converted to **2** upon heating at 70°C over 2 months (Figure S39), however. We thus infer that **2** is the thermodynamically favored product even at low concentrations, with **3** being an isolable kinetic product.

Design principles driving the formation of capsule 2

Capsule **2**, with its faces paneled by three ligands, is much larger than capsule **3**, in which the faces of the cube-like architecture are paneled by single ligand units. Within **2**, the mean Zn···Zn distance between the *fac* Zn^{II} vertices is 31.8 ± 0.2 Å, whereas in **3**, the mean Zn···Zn distance between corners is 14.2 ± 0.2 Å. The volumes of the interior cavities of **2** and **3** were calculated to be 5,340 and 852 $Å^3$, respectively, using the VOIDOO program.[35] Given that **2** contains twice as many components as **3** and has an internal volume almost an order of magnitude greater than that of **3**, we infer there to be a strong enthalpic driving force for the formation of **2** to overcome the likely entropic penalty.

The biphenyl core of tetra-aniline subcomponent **1** provides conformational flexibility. The geometry of cube-like species **3** requires all four bidentate sites of the ligand to lie in the same plane, leading to the small observed mean dihedral angle of 5.8° ± 2.5° between the two phenyl rings of the central biphenyl unit (Figure 3). In contrast, a wider mean torsion angle of 30.2° ± 5.4° was observed in **2**. The greater biphenyl torsion of **2** avoids the enthalpic penalty associated with eclipsing the four central hydrogen atoms of the biphenyl unit within **3**.

Two design principles to drive the formation of **2** are elucidated in considering the structures of **2** and **3**. First, the preference for subcomponent **1** to adopt a twisted conformation is accommodated in **2** but suppressed in **3**. Second, the rectangular structure of **1** may introduce strain into the cuboidal architecture of **3**, where each pair of vertices forms the junction between the long axis of one ligand and the short axis of another. The extended framework of **2**, in contrast, brings short and long axes together only around the *fac* Zn^{II} vertices, with a mean Zn···Zn distance of 14.6 ± 0.2 Å, similar to 14.2 ± 0.2 Å observed in **3**. Pairs of *mer* vertices match short with short axes (mean Zn···Zn distance: 10.2 ± 0.1 Å) and bridge the edges of the four triangular pores of the structure with long axes (mean Zn···Zn distance: 15.5 ± 0.1 Å). Such a configuration may result in diminished strain overall within **2**. The first principle, the preference for **1** to adopt a twisted conformation, appears to play an essential role in driving the formation of **2**: Rectangular subcomponents with the ability, but no thermodynamic preference, to twist have been observed only to form smaller M_8L_6 architectures.[29,31]

Encapsulation of multiple equivalents of $Mo_6O_{19}^{2-}$ within 2

The screening of a series of prospective guests (Section S2.3) revealed that **2** bound $Mo_6O_{19}^{2-}$ (hexamolybdate, Figure 4A). The progressive addition of $(^nBu_4N)_2Mo_6O_{19}$ to a solution of **2** in acetonitrile led to the appearance of multiple new signals. After the addition of 6 equiv of $(^nBu_4N)_2Mo_6O_{19}$, the ^{1}H NMR spectrum simplified to the one having the same number of signals as the original sample of **2**, but many signals were shifted from their original chemical shift values (Figure S30). ^{1}H DOSY data indicated that all of these signals had a similar diffusion coefficient to the signals for **2** (Figure S37), further consistent with the hypothesis of host-guest binding, as opposed to structural rearrangement.

The 5,340 $Å^3$ cavity of **2** is large enough to bind more than 1 equiv of $Mo_6O_{19}^{2-}$, having a van der Waals volume of 299 $Å^3$, as calculated using BIOVIA Discovery Studio Visualizer.[37] We infer that below 6 equiv of hexamolybdate (Figure 4B), the complex ^{1}H NMR spectra are due to the presence of host-guest species with differing numbers of guests bound. This spectral complexity precluded quantification of the binding affinities for the different $Mo_6O_{19}^{2-}$ adducts of **2**. The simplification of the ^{1}H NMR spectrum after the addition of 6 equiv of hexamolybdate indicates convergence to a single host-guest species, where one host binds between 3 and 5 equiv of hexamolybdate. Further discussion can be found in Section S2.1. No interaction between cube-like architecture **3** and $Mo_6O_{19}^{2-}$ was observed by ^{1}H NMR spectroscopy, however, and $Mo_6O_{19}^{2-}$ was instead observed to accelerate the conversion of **3** to **2** (Figures S40 and S41).

Conclusions

A large metal-organic capsule **2** assembled from a simple twisted tetramine subcomponent, with three tetramine residues paneling each face of the polyhedral capsule. The process by which **2** assembles, resembling that of natural protein capsids, and its ability to bind guests, set it apart from the other largest metal-organic polyhedra.[8–14,17–19] The self-assembly rules followed by the system reported in generating capsule **2** as the thermodynamic product, as opposed to the smaller cuboid

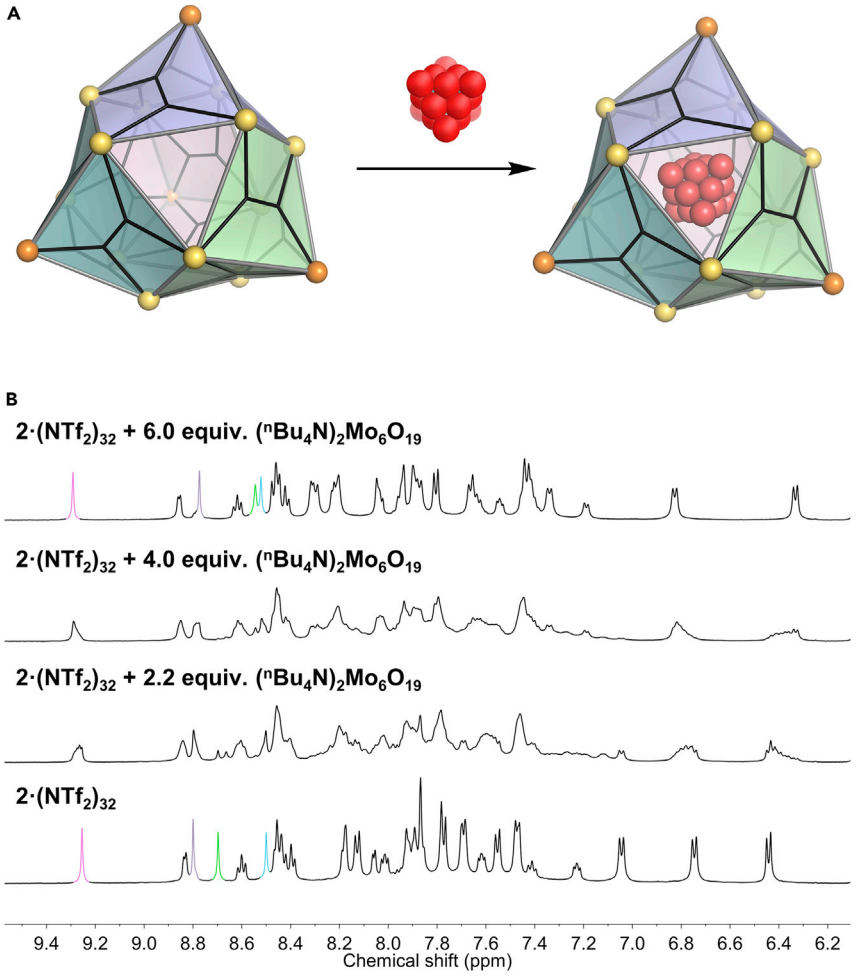

Figure 4. Host-guest chemistry within 2

(A) Schematic showing the binding of $Mo_6O_{19}^{2-}$ (shown in red)[36] by **2**; multiple $Mo_6O_{19}^{2-}$ bind within **2** but only 1 equiv is shown for clarity.

(B) ^{1}H NMR spectra (500 MHz, CD_3CN, 298 K) showing the spectral changes during the progressive titration of $(^nBu_4N)_2Mo_6O_{19}$ into a solution of **2**·$(NTf_2)_{32}$.

3, may be of more general use. Future work will thus explore how the twist and aspect ratio of tetramines analogous to **1** influences their tendency to assemble into higher-order structures. Virus capsids show how increasing the number of protein subunits that span polyhedral vertices can lead to large, higher-order members of the set of Goldberg polyhedra.[1–3,26,27] Extension of the concepts elucidated herein may enable the preparation of synthetic capsules that are enlarged through the incorporation of more subunits spanning vertices, as well as $M_{16}L_{12}$ capsules containing larger individual ligands. Future work will explore the origins of the energetic difference between structures **2** and **3** through calculations, which may inform these future attempts to generate larger structures. Such capsules may become useful in the binding of much larger cargoes than is currently possible, including proteins and oligonucleotides, as with their natural congeners. Furthermore, replacement of the hydrogen atom at the 3-position of the 2-formylpyridine subcomponent could allow for the functionalization of the $M_{16}L_{12}$ framework at both inward-facing and outward-facing positions, allowing the modification of the properties of the internal cavity, degree of enclosure, and solubility preferences of the structure (Figure S50).

EXPERIMENTAL PROCEDURES

Full experimental procedures can be found in the supplemental information.

Resource availability

Lead contact

Further information and requests for resources and reagents should be directed to the lead contact, Jonathan R. Nitschke (jrn34@cam.ac.uk).

Materials availability

This study did not generate unique reagents.

Data and code availability

All data supporting the findings of this study are included within the article and its supplemental information and are also available from the authors upon request. Crystallographic data for the structures reported in this paper have been deposited at the Cambridge Crystallographic Data Centre, under the deposition numbers CCDC:2104915 (**2**) and CCDC:2104916 (**3**). Copies of these data can be obtained free of charge via www.ccdc.cam.ac.uk/data_request/cif.

SUPPLEMENTAL INFORMATION

Supplemental information can be found online at https://doi.org/10.1016/j.chempr.2022.01.003.

ACKNOWLEDGMENTS

This study was supported by the European Research Council (695009) and the UK Engineering and Physical Sciences Research Council (EP/P027067/1 and EP/T031603/1). The authors also thank Diamond Light Source (UK) for synchrotron beamtime on I19 (CY21497), the NMR service in the Yusuf Hamied Department of Chemistry at the University of Cambridge for NMR experiments, and the group of Professor P. A. Gale for providing $(^{n}Bu_4N)_2Mo_6O_{19}$. We thank Andrew Tarzia and Kim Jelfs for preliminary DFT calculations to compare the energies of **2** and **3**.

AUTHOR CONTRIBUTIONS

J.R.N. and J.A.D. conceived the study, analyzed the results, and wrote the manuscript. Experiments were performed by J.A.D. T.K.R refined the X-ray crystallographic data. All authors discussed the results and edited the manuscript.

DECLARATION OF INTERESTS

The authors declare no competing interests.

Received: September 30, 2021
Revised: November 18, 2021
Accepted: January 6, 2022
Published: February 1, 2022

REFERENCES

1. Aumiller, W.M., Uchida, M., and Douglas, T. (2018). Protein cage assembly across multiple length scales. Chem. Soc. Rev. *47*, 3433–3469. https://doi.org/10.1039/C7CS00818J.

2. Prasad, B.V.V., Hardy, M.E., Dokland, T., Bella, J., Rossmann, M.G., and Estes, M.K. (1999). X-ray crystallographic structure of the Norwalk virus capsid. Science *286*, 287–290. https://doi.org/10.1126/science.286.5438.287.

3. Mateu, M.G. (2013). Assembly, stability and dynamics of virus capsids. Arch. Biochem. Biophys. *531*, 65–79. https://doi.org/10.1016/j.abb.2012.10.015.

4. Chakrabarty, R., Mukherjee, P.S., and Stang, P.J. (2011). Supramolecular coordination: self-assembly of finite two- and three-dimensional ensembles. Chem. Rev. *111*, 6810–6918. https://doi.org/10.1021/cr200077m.

5. Ward, M.D., Hunter, C.A., and Williams, N.H. (2018). Coordination cages based on

bis(pyrazolylpyridine) ligands: structures, dynamic behavior, guest binding, and catalysis. Acc. Chem. Res. *51*, 2073–2082. https://doi.org/10.1021/acs.accounts.8b00261.

6. Zhang, D., Ronson, T.K., and Nitschke, J.R. (2018). Functional capsules via subcomponent self-assembly. Acc. Chem. Res. *51*, 2423–2436. https://doi.org/10.1021/acs.accounts.8b00303.

7. Liu, W., and Stoddart, J.F. (2021). Emergent behavior in nanoconfined molecular containers. Chem *7*, 919–947. https://doi.org/10.1016/j.chempr.2021.02.016.

8. Sun, Q.-F., Iwasa, J., Ogawa, D., Ishido, Y., Sato, S., Ozeki, T., Sei, Y., Yamaguchi, K., and Fujita, M. (2010). Self-assembled $M_{24}L_{48}$ polyhedra and their sharp structural switch upon subtle ligand variation. Science *328*, 1144–1147. https://doi.org/10.1126/science.1188605.

9. Fujita, D., Ueda, Y., Sato, S., Yokoyama, H., Mizuno, N., Kumasaka, T., and Fujita, M. (2016). Self-assembly of $M_{30}L_{60}$ Icosidodecahedron. Chem *1*, 91–101. https://doi.org/10.1016/j.chempr.2016.06.007.

10. Fujita, D., Ueda, Y., Sato, S., Mizuno, N., Kumasaka, T., and Fujita, M. (2016). Self-assembly of tetravalent Goldberg polyhedra from 144 small components. Nature *540*, 563–566. https://doi.org/10.1038/nature20771.

11. Olenyuk, B., Whiteford, J.A., Fechtenkötter, A., and Stang, P.J. (1999). Self-assembly of nanoscale cuboctahedra by coordination chemistry. Nature *398*, 796–799. https://doi.org/10.1038/19740.

12. Olenyuk, B., Levin, M.D., Whiteford, J.A., Shield, J.E., and Stang, P.J. (1999). Self-assembly of nanoscopic dodecahedra from 50 predesigned components. J. Am. Chem. Soc. *121*, 10434–10435. https://doi.org/10.1021/ja9931933.

13. Xie, T.-Z., Guo, K., Guo, Z., Gao, W.-Y., Wojtas, L., Ning, G.-H., Huang, M., Lu, X., Li, J.-Y., Liao, S.-Y., et al. (2015). Precise molecular fission and fusion: quantitative self-assembly and chemistry of a metallo-cuboctahedron. Angew. Chem. Int. Ed. Engl. *54*, 9224–9229. https://doi.org/10.1002/anie.201503609.

14. Wang, H., Wang, K., Xu, Y., Wang, W., Chen, S., Hart, M., Wojtas, L., Zhou, L.-P., Gan, L., Yan, X., et al. (2021). Hierarchical self-assembly of nanowires on the surface by metallo-supramolecular truncated cuboctahedra. J. Am. Chem. Soc. *143*, 5826–5835. https://doi.org/10.1021/jacs.1c00625.

15. Bilbeisi, R.A., Ronson, T.K., and Nitschke, J.R. (2013). A self-assembled $[Fe^{II}_{12}L_{12}]$ capsule with an icosahedral framework. Angew. Chem. Int. Ed. Engl. *52*, 9027–9030. https://doi.org/10.1002/anie.201302976.

16. Rizzuto, F.J., and Nitschke, J.R. (2017). Stereochemical plasticity modulates cooperative binding in a $Co^{II}_{12}L_6$ cuboctahedron. Nat. Chem. *9*, 903–908. https://doi.org/10.1038/nchem.2758.

17. Pasquale, S., Sattin, S., Escudero-Adán, E.C., Martínez-Belmonte, M., and de Mendoza, J. (2012). Giant regular polyhedra from calixarene carboxylates and uranyl. Nat. Commun. *3*, 785. https://doi.org/10.1038/ncomms1793.

18. Chen, Y.-S., Solel, E., Huang, Y.-F., Wang, C.-L., Tu, T.-H., Keinan, E., and Chan, Y.-T. (2019). Chemical mimicry of viral capsid self-assembly via coranulene-based pentatopic tectons. Nat. Commun. *10*, 3443. https://doi.org/10.1038/s41467-019-11457-6.

19. Liu, D., Chen, M., Li, K., Li, Z., Huang, J., Wang, J., Jiang, Z., Zhang, Z., Xie, T., Newkome, G.R., and Wang, P. (2020). Giant truncated metallo-tetrahedron with unexpected supramolecular aggregation induced emission enhancement. J. Am. Chem. Soc. *142*, 7987–7994. https://doi.org/10.1021/jacs.0c02366.

20. Koo, J., Kim, I., Kim, Y., Cho, D., Hwang, I.-C., Mukhopadhyay, R.D., Song, H., Ko, Y.H., Dhamija, A., Lee, H., et al. (2020). Gigantic porphyrinic cages. Chem *6*, 3374–3384. https://doi.org/10.1016/j.chempr.2020.10.002.

21. Zhang, G., Presly, O., White, F., Oppel, I.M., and Mastalerz, M. (2014). A Permanent mesoporous organic cage with an exceptionally high surface area. Angew. Chem. Int. Ed. Engl. *53*, 1516–1520. https://doi.org/10.1002/anie.201308924.

22. Ono, K., Johmoto, K., Yasuda, N., Uekusa, H., Fujii, S., Kiguchi, M., and Iwasawa, N. (2015). Self-assembly of nanometer-sized boroxine cages from diboronic acids. J. Am. Chem. Soc. *137*, 7015–7018. https://doi.org/10.1021/jacs.5b02716.

23. Sehnal, D., Bittrich, S., Deshpande, M., Svobodová, R., Berka, K., Bazgier, V., Velankar, S., Burley, S.K., Koča, J., and Rose, A.S. (2021). Mol* Viewer: modern web app for 3D visualization and analysis of large biomolecular structures. Nucleic Acids Res *49*, W431–W437. https://doi.org/10.1093/nar/gkab314.

24. Johnson, E., Cascio, D., Sawaya, M.R., Gingery, M., and Schröder, I. (2005). Crystal structures of a tetrahedral open pore ferritin from the hyperthermophilic archaeon *Archaeoglobus fulgidus*. Structure *13*, 637–648. https://doi.org/10.1016/j.str.2005.01.019.

25. Berman, H.M., Westbrook, J., Feng, Z., Gilliland, G., Bhat, T.N., Weissig, H., Shindyalov, I.N., and Bourne, P.E. (2000). The Protein Data Bank. Nucleic Acids Res *28*, 235–242. https://doi.org/10.1093/nar/28.1.235.

26. Zandi, R., Reguera, D., Bruinsma, R.F., Gelbart, W.M., and Rudnick, J. (2004). Origin of icosahedral symmetry in viruses. Proc. Natl. Acad. Sci. USA *101*, 15556–15560. https://doi.org/10.1073/pnas.0405844101.

27. Twarock, R., and Luque, A. (2019). Structural puzzles in virology solved with an overarching icosahedral design principle. Nat. Commun. *10*, 4414. https://doi.org/10.1038/s41467-019-12367-3.

28. Wu, T., Jiang, Z., Bai, Q., Li, Y., Mao, S., Yu, H., Wojtas, L., Tang, Z., Chen, M., Zhang, Z., et al. (2021). Supramolecular triangular orthobicupola: self-assembly of a giant Johnson solid J27. Chem *7*, 2429–2441. https://doi.org/10.1016/j.chempr.2021.06.003.

29. Jiao, J., Li, Z., Qiao, Z., Li, X., Liu, Y., Dong, J., Jiang, J., and Cui, Y. (2018). Design and self-assembly of hexahedral coordination cages for cascade reactions. Nat. Commun. *9*, 4423. https://doi.org/10.1038/s41467-018-06872-0.

30. Gong, Y., Qin, C., Zhang, Y., Sun, C., Pan, Q., Wang, X., and Su, Z. (2020). Face-directed assembly of molecular cubes: in situ substitution of a predetermined concave cluster. Angew. Chem. Int. Ed. Engl. *59*, 22034–22038. https://doi.org/10.1002/anie.202010824.

31. Yang, L., Jing, X., He, C., Chang, Z., and Duan, C. (2016). Redox-active M_8L_6 cubic hosts with tetraphenylethylene faces encapsulate organic dyes for light-driven H_2 production. Chem. Eur. J. *22*, 18107–18114. https://doi.org/10.1002/chem.201601447.

32. Pang, J., Yuan, S., Qin, J., Liu, C., Lollar, C., Wu, M., Yuan, D., Zhou, H.-C., and Hong, M. (2017). Control the structure of Zr-tetracarboxylate frameworks through steric tuning. J. Am. Chem. Soc. *139*, 16939–16945. https://doi.org/10.1021/jacs.7b09973.

33. Sham, K.-C., Yiu, S.-M., and Kwong, H.-L. (2013). Dodecanuclear hexagonal-prismatic $M_{12}L_{18}$ coordination cages by subcomponent self-assembly. Inorg. Chem. *52*, 5648–5650. https://doi.org/10.1021/ic400665m.

34. Grant, R.A., Filman, D.J., Finkel, S.E., Kolter, R., and Hogle, J.M. (1998). The crystal structure of Dps, a ferritin homolog that binds and protects DNA. Nat. Struct. Biol. *5*, 294–303. https://doi.org/10.1093/nar/28.1.235.

35. Kleywegt, G.J., and Jones, T.A. (1994). Detection, delineation, measurement and display of cavities in macromolecular structures. Acta Crystallogr. D Biol. Crystallogr. *50*, 178–185. https://doi.org/10.1107/S0907444993011333.

36. Clegg, W., Sheldrick, G.M., Garner, C.D., and Walton, I.B. (1982). Structure of bis(tetraphenylarsonium) hexamolybdate(VI). Acta Crystallogr. B Struct. Sci. *38*, 2906–2909. https://doi.org/10.1107/S0567740882010292.

37. Discovery Studio Visualizer v21.1.0.20298, Copyright 2020 Dassault Systèmes Biovia Corp.